MITSUBISHI ELECTRIC RESEARCH LABORATORIES
https://www.merl.com

Fail-safe Rendezvous Control on Elliptic Orbits using Reachable Sets

Aguilar Marsillach, Daniel; Di Cairano, Stefano; Weiss, Avishai

TR2020-098 July 03, 2020

Abstract

In this paper, a fail-safe control policy is developed for rendezvous on generic elliptic orbits using backwards reachable sets and model predictive control (MPC). The backwards reachable sets are computed as unsafe regions of state space that, in the event of total thruster failure, would lead to a collision between the chaser spacecraft and the rendezvous target. The backwards reachable sets are incorporated as passive safety constraints in the MPC online trajectory generation in order to guide the chaser to rendezvous with its target through an inherently safe approach. Simulations demonstrate the effectiveness of the passive safety constraints in altering a nominally unsafe rendezvous to one that is passively safe.

American Control Conference (ACC) 2020

Mitsubishi Electric Research Laboratories, Inc.
201 Broadway, Cambridge, Massachusetts 02139

Fail-safe Rendezvous Control on Elliptic Orbits using Reachable Sets

Daniel Aguilar Marsillach[1], Stefano Di Cairano[2], Avishai Weiss[3]

***Abstract*— In this paper, a fail-safe control policy is developed for rendezvous on generic elliptic orbits using backwards reachable sets and model predictive control (MPC). The backwards reachable sets are computed as unsafe regions of state space that, in the event of total thruster failure, would lead to a collision between the chaser spacecraft and the rendezvous target. The backwards reachable sets are incorporated as passive safety constraints in the MPC online trajectory generation in order to guide the chaser to rendezvous with its target through an inherently safe approach. Simulations demonstrate the effectiveness of the passive safety constraints in altering a nominally unsafe rendezvous to one that is passively safe.**

I. INTRODUCTION

A critical criteria for spacecraft rendezvous is the maintenance of passive safety [1], that is, the ability to avoid a collision between a chaser spacecraft and its target in the event of a complete loss of control. Passive safety is imperative as it impedes the necessity for collision avoidance maneuvers until much later in the approach. This not only saves fuel but also provides safety with respect to worst-case spacecraft navigation and control failures. Typically, classic approaches guarantee passive safety through the trajectory generation process, completed in open-loop. Recent advances have been made in online generation of passively safe trajectories by using convex and non-convex constraints in a receding-horizon control strategy [2], [3]. In [4] a guidance and control strategy for spacecraft swarms is developed using relative orbital elements, yielding passively safe and bounded relative motion.

An alternative approach to verify the safety of a system is the concept of reachability, which aims to compute the exact or approximate set of states that can be reached by a system, given initial or final states, a time-horizon, inputs, and the model parameters. For linear systems, sets can be represented using n-dimensional geometric objects such as zonotopes [5] , polyhedra [6], or ellipsoids [7]. Such representations are useful for linear systems because they are closed under affine transformations [8]. For nonlinear systems, a variety of analyses can be performed. In [5] the nonlinear dynamics are approximated to a given order and the approximation error is used to inflate zonotope sets. Another method uses optimal control to solve the Hamilton-Jacobi partial differential equation to compute reachable sets, but remains computationally intractable for high dimensional systems [9]. Reachable sets can also be approximated by sampling the initial or final set boundary and solving optimal control problems [10].

Reachability has been used in prior work related to spacecraft rendezvous and docking to verify the viability and safety of an active control strategy. In [11] backwards reachable sets using the linear time-invariant (LTI) Clohessey-Wiltshire (CW) equations, that describe the relative motion dynamics on a circular orbit, are used to determine which initial conditions lead to a successful docking maneuver. The work in [12] computes reach-avoid sets to obtain trajectories that reach the target while avoiding a line-of-sight set, whereas [12], [13] focus on stochastic reachable set computation, and then use the constructed sets for a spacecraft rendezvous and docking simulation [14].

In this work, we combine concepts from reachability and receding-horizon control to design an online trajectory generation algorithm that produces passively safe rendezvous trajectories for a chaser spacecraft to its target on generic elliptic orbits. For achieving passive safety, we compute the backwards reachable set over a time interval (BRSI) from the target to determine the regions of state space corresponding to unsafe areas in which, in the absence of control, a chaser spacecraft would collide with the target within a specified time-horizon. For computational tractability, we linearize the nonlinear relative equations of motion about the target's generic orbit, resulting in a set of linear time-varying (LTV) equations. Due to the LTV nature of the system, exact computation of the BRSI is impossible [15], hence we conservatively approximate the unsafe region with offline computation of the union of BRSI along the target's entire orbit. The union of BRSI determines the region to be avoided, which is formulated as passive safety constraints for the online trajectory generation process. We develop a model predictive control (MPC) policy that enforces the constraints, thus ensuring that the spacecraft remains outside of the union of BRSI, and hence guaranteeing collision free trajectories in the event of thruster failure. MPC has previously been applied for spacecraft rendezvous under nominal propulsion conditions, see [16]–[18] and references therein, however, passive safety was never addressed.

The proposed approach is applied to a mission staged into three phases. The first phase constrains the controller to maintain passive safety with respect to an approach ellipsoid (AE) around the target. Once the command to enter the AE is issued, the second phase maintains passive safety with respect to a keep-out ellipsoid (KOE). Finally, once the final approach is engaged, the chaser spacecraft may enter the KOE, at which point passive safety is no longer enforced.

[1] D. Aguilar Marsillach is with the Department of Aerospace Engineering Sciences at the University of Colorado - Boulder, Boulder, CO 80303, USA. Email: d.aguilar@colorado.edu. He interned at MERL during the development of this work.

[2,3] A. Weiss and S. Di Cairano are with Mitsubishi Electric Research Laboratories, Cambridge, MA 02139, USA. Emails: {weiss,dicairano}@merl.com

Fig. 1 provides an illustration of the AE and KOE, and a backwards reach set projected onto the orbital frame.

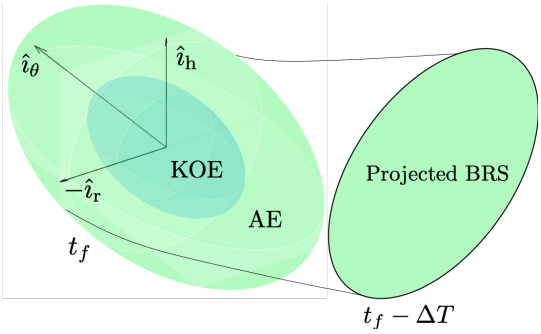

Fig. 1. Representation of backward reachable set projected onto the target orbital frame. Approach ellipsoid (AE) in green, the keep-out ellipsoid (KOE) in light blue.

II. Spacecraft Model

Consider a target and a chaser in orbit around Earth. The frame $\mathrm{F_e}$ is the Earth-Centered Inertial (ECI) frame, e is an unforced particle, and it is assumed that e is collocated with the center of the Earth. The chaser's center of mass is denoted by c and has a chaser-fixed frame $\mathrm{F_c}$. The target's center of mass is denoted by t and has a target-fixed frame $\mathrm{F_t}$. In this work we assume the target is aligned with its orbital frame such that it has the radial, along-track, and cross-track basis vectors: $\mathrm{F_t} = \{\hat{\imath}_r, \hat{\imath}_\theta, \hat{\imath}_h\}$. A derivative with respect to the inertial frame is denoted by ${}^{\mathrm{e}}(\dot{\cdot})$ whereas a derivative with respect to another frame is denoted by $(\dot{\cdot})$. The target orbital frame's angular velocity with respect to the inertial frame is $\omega_{\mathrm{t/e}}$. Both the target and chaser's bodies are assumed to be rigid and all external forces acting on the spacecraft are assumed to act on the center of mass of their respective bodies.

The translational equations of motion for the target and chaser relative to the inertial frame $\mathrm{F_e}$ are given by

$$ {}^{\mathrm{e}}\ddot{\mathbf{r}}_\mathrm{t} = -\mu \frac{\mathbf{r}_\mathrm{t}}{||\mathbf{r}_\mathrm{t}||^3} + \frac{\mathbf{f}_\mathrm{t}}{m_\mathrm{t}}, \tag{1} $$

$$ {}^{\mathrm{e}}\ddot{\mathbf{r}}_\mathrm{c} = -\mu \frac{\mathbf{r}_\mathrm{c}}{||\mathbf{r}_\mathrm{c}||^3} + \frac{\mathbf{f}_\mathrm{c}}{m_\mathrm{c}} \tag{2} $$

where $\mathbf{r}_\mathrm{t}, \mathbf{r}_\mathrm{c}$ are the position vectors of the target and chaser center of mass relative to the center of their central body, $m_\mathrm{t}, m_\mathrm{c}$ are the target and chaser masses, μ is the gravitational constant of the central body, and $\mathbf{f}_\mathrm{t}$, $\mathbf{f}_\mathrm{c}$ represent perturbing forces acting on the target and chaser, respectively. These perturbations include orbital perturbations as well as control. In this study, the target is assumed to follow Keplerian motion, i.e. $\mathbf{f}_\mathrm{t} = \mathbf{0}$, and we neglect orbital perturbations on the chaser.

Given a target and chaser, the relative distance between their centers of mass is given by

$$ \mathbf{r}_\mathrm{rel} = \mathbf{r}_\mathrm{c} - \mathbf{r}_\mathrm{t} = \begin{bmatrix} \delta x & \delta y & \delta z \end{bmatrix}^\mathsf{T}. \tag{3} $$

For the purposes of rendezvous, it is of interest to resolve relative positions and velocities of the chaser in the target's orbital frame. Taking the derivative of the relative position (3) with respect to the target's orbital frame $\mathrm{F_t}$ yields

$$ \dot{\mathbf{r}}_\mathrm{rel} = {}^{\mathrm{e}}\dot{\mathbf{r}}_\mathrm{t} - {}^{\mathrm{e}}\dot{\mathbf{r}}_\mathrm{c} - \omega_{\mathrm{t/e}} \times \mathbf{r}_\mathrm{rel}. \tag{4} $$

Taking the derivative of the relative velocity (4) with respect to the target's orbital frame $\mathrm{F_t}$ yields

$$ \ddot{\mathbf{r}}_\mathrm{rel} = {}^{\mathrm{e}}\ddot{\mathbf{r}}_\mathrm{t} - {}^{\mathrm{e}}\ddot{\mathbf{r}}_\mathrm{c} - \dot{\omega}_{\mathrm{t/e}} \times \mathbf{r}_\mathrm{rel} + \omega_{\mathrm{t/e}} \times (\omega_{\mathrm{t/e}} \times \mathbf{r}_\mathrm{rel}) - 2\omega_{\mathrm{t/e}} \times \dot{\mathbf{r}}_\mathrm{rel}. \tag{5} $$

Finally, substituting (1), (2) into (5) yields the full nonlinear relative equations of motion. For

$$ ||\mathbf{r}_\mathrm{rel}|| << ||\mathbf{r}_\mathrm{t}||, \tag{6} $$

the equations of relative motion (5) can be linearized with respect to the target's trajectory, yielding [19]

$$ \begin{aligned} \delta\ddot{x} - \left(\tfrac{2\mu}{r_\mathrm{t}^3} + \tfrac{h^2}{r_\mathrm{t}^4}\right)\delta x + \left(\tfrac{2\,{}^{\mathrm{e}}\dot{\mathbf{r}}_\mathrm{t}^\top \mathbf{r}_\mathrm{t}}{r_\mathrm{t}^4} h\right)\delta y - \left(\tfrac{2h}{r_\mathrm{t}^2}\right)\delta\dot{y} &= \tfrac{u_1}{m_\mathrm{c}}, \\ \delta\ddot{y} + \left(\tfrac{\mu}{r_\mathrm{t}^3} - \tfrac{h^2}{r_\mathrm{t}^4}\right)\delta y - \left(\tfrac{2\,{}^{\mathrm{e}}\dot{\mathbf{r}}_\mathrm{t}^\top \mathbf{r}_\mathrm{t}}{r_\mathrm{t}^4} h\right)\delta x + \left(\tfrac{2h}{r_\mathrm{t}^2}\right)\delta\dot{x} &= \tfrac{u_2}{m_\mathrm{c}}, \\ \delta\ddot{z} + \left(\tfrac{\mu}{r_\mathrm{t}^3}\right)\delta z &= \tfrac{u_3}{m_\mathrm{c}}, \end{aligned} \tag{7} $$

where $r_\mathrm{t} = ||\mathbf{r}_\mathrm{t}||$, $h = ||\mathbf{r}_\mathrm{t} \times {}^{\mathrm{e}}\dot{\mathbf{r}}_\mathrm{t}||$ is the inertial specific angular momentum of the target's orbit, and $\mathbf{f}_\mathrm{c} = \begin{bmatrix} u_1 & u_2 & u_3 \end{bmatrix}^\mathsf{T}$ is the control input applied to the chaser.

The linear time-varying equations of motion (7) are written in state space form as

$$ \dot{\mathbf{x}}(t) = A(t)\mathbf{x}(t) + B\mathbf{u}(t), \tag{8} $$

where $\mathbf{x} = \begin{bmatrix} \delta x & \delta y & \delta z & \delta\dot{x} & \delta\dot{y} & \delta\dot{z} \end{bmatrix}^\mathsf{T}$, and $\mathbf{u} = \mathbf{f}_\mathrm{c}$. For simplifying computations, we consider a discrete time formulation of (8) obtained by sampling with period Δt,

$$ \mathbf{x}_{t+1} = f(t, x_t, u_t) = A_d(t)\mathbf{x}_t + B_d(t)\mathbf{u}_t. \tag{9} $$

The homogeneous solution of (9), i.e., $\mathbf{u}_t = 0$ for all t, will be used in the next section to compute backwards reachable sets for passive safety.

III. Reachable Sets and Passive Safety

For passive safety, we compute backward reachable sets (BRS) under no control input, $\mathbf{u}_t = 0$ for all t, of a final ellipsoidal set. Given a target set $\mathcal{S}_f$ and a target time t_f, the backward reachable set under no control action from $t_j \leq t_f$ to t_f is defined recursively by [6]

$$ \mathcal{R}_b(t_f; \mathcal{S}_f, t_f) = \mathcal{S}_f, \tag{10a} $$

$$ \begin{aligned} \mathcal{R}_b(t_{j-1}; \mathcal{S}_f, t_f) = \{\mathbf{x} \in \mathbb{R}^n : \\ f(t_{j-1}, \mathbf{x}, \mathbf{0}) \in \mathcal{R}_b(t_j; \mathcal{S}_f, t_f)\}, \end{aligned} \tag{10b} $$

where $\mathcal{R}_b(t_j; \mathcal{S}_f, t_f)$ describes the set of all the states at t_j that end up in $\mathcal{S}_f$ at t_f without any control. We define the backwards reachable set over a time interval (BRSI) as the union of all BRS in the time-interval $[t, t_f]$

$$ \tilde{\mathcal{R}}_{[t,t_f]}(t; S_f, t_f) = \bigcup_{\tau=t}^{t_f} \mathcal{R}_b(\tau; S_f, t_f). \tag{11} $$

A. Ellipsoidal Set Representations

In this paper we consider the target set $\mathcal{S}_f$ to be represented by ellipsoids. An ellipsoid centered at $\mathbf{d} \in \mathbb{R}^n$ with shape matrix D, is defined as [7], [20]

$$\mathcal{E}(\mathbf{d}, D) \triangleq \{\mathbf{x} \in \mathbb{R}^n \ : \ (\mathbf{x}-\mathbf{d})^\top D^{-1}(\mathbf{x}-\mathbf{d}) \leq 1\}. \quad (12)$$

Ellipsoids are closed under affine transformations. Given $\mathcal{E}(\mathbf{d}, D)$, $A \in \mathbb{R}^{n\times n}$ and $\mathbf{b} \in \mathbb{R}^{n\times 1}$

$$A\mathcal{E}(\mathbf{d}, D) + \mathbf{b} = \mathcal{E}(A\mathbf{d}+\mathbf{b}, ADA^\top). \quad (13)$$

The AE and KOE are ellipsoids centered at $\mathbf{d} = \mathbf{0}$, with shape matrix P at time t_f, such that

$$\mathcal{S}_f = \{\mathbf{x} \in \mathbb{R}^6, \ \mathbf{x}^\top P^{-1}\mathbf{x} \leq 1\}, \quad (14)$$

where the shape matrices for the AE and KOE are $P = \{P_{\mathrm{AE}}, P_{\mathrm{KOE}}\}$.

Since $\mathcal{S}_f$ are ellipsoids and the discrete-time dynamics (9) are linear time-varying, with $\mathbf{u}(t) = 0$, the BRS (10) are also ellipsoids. In fact, given the ellipsoidal final set (14) and defining for the sake of simplicity the t_j-to-t_h state transition matrix[1] $\Phi(t_h, t_j) = \Pi_{i=j}^{h} A_d(t_i)$, the BRS is

$$\mathcal{R}(t_k; \mathcal{S}_f, t_f) = \{\mathbf{x} \in \mathbb{R}^n : \mathbf{x}^\top \Phi(t_f, t_k)^\top \ P^{-1} \ \Phi(t_f, t_k) \ \mathbf{x} \leq 1\}. \quad (15)$$

B. Union of BRSI

Given the ellipsoidal final set (14), defined by a shape matrix P, the N-step BRSI is defined as

$$\tilde{\mathcal{R}}_{[t_f-N, t_f]}(t_f - N; \mathcal{S}_f, t_f) = \bigcup_{t_i = t_f - N}^{t_f} \{\mathbf{x} \in \mathbb{R}^n \ : \ \mathbf{x}^\top \Phi(t_f, t_i)^\top \ P^{-1} \ \Phi(t_f, t_i) \ \mathbf{x} \leq 1\}, \quad (16)$$

The BRSI (16) is not an ellipsoid, but it is the union of a finite set of ellipsoids.

Due to the LTV nature of the dynamics, the BRSI vary across different portions of the target's orbit. Hence, to maintain safety for a duration on the order of an orbital period, or higher, several BRSI are computed with respect to numerous target sets along the target's orbit. Computing the N-step BRSI given $\mathbf{r}_{\mathrm{t}}$ results in a discrete-time representation[2] of the N-step BRSI of the LTV system. The approximation of the full LTV BRSI is obtained by taking the union of such sets,

$$\bar{\mathcal{R}}(t_k; \mathcal{S}_f, t_f) = \bigcup_{t_f = t_p+1}^{2t_p} \bigcup_{t_k = t_f - N}^{t_f} \{\mathbf{x} \in \mathbb{R}^n \ : \ \mathbf{x}^\top \Phi(t_f, t_k)^\top P^{-1} \Phi(t_f, t_k) \mathbf{x} \leq 1\}, \quad (17)$$

[1]Even if not stated explicitly, matrices with larger step indices are added to the left, as matrix product is not commutative.

[2]All discrete time representations of BRS and BRSI are in fact approximations for the actual system behavior that is continuous-time, yet some approximations are necessary for the case of time varying systems [21]. However, these approximations can be made sufficiently accurate by an appropriate choice of the sampling period Δt.

where t_p is the orbital period of the target and we have assumed $N\Delta t << t_p$. The union operator on the left ensures the target state is evaluated at discrete points along an orbital period, yielding a set of final states

$$X_f = \{\mathbf{x}(t_f), \ \mathbf{x}(t_f + \Delta T), \ \ldots, \ \mathbf{x}(t_f + t_p)\}, \quad (18)$$

which is equivalent to evaluating $\mathbf{r}_{\mathrm{t}}$, ${}^{\mathrm{e}}\dot{\mathbf{r}}_{\mathrm{t}}$ at different true anomalies $\theta \in [0, 2\pi]$, since $t \propto \theta$. The BRSI (17) ensures safety for a time horizon N from the current time.

C. Passive Safety

Passive safety ensures that with natural free-drift dynamics, the chaser spacecraft does not intersect the AE or KOE in the event of total control loss. Safety is defined only by the relative position; the velocity at which the chaser spacecraft enters the AE or KOE is immaterial. As such, the shape matrix P is defined as a degenerate ellipsoid with unbounded velocity minor/major axes. Thus, $P_{\{\mathrm{AE,KOE}\}}$ is a rank deficient shape matrix

$$P_{\{\mathrm{AE,KOE}\}} = \begin{bmatrix} P_{\mathrm{p}} & 0_{3\times 3} \\ 0_{3\times 3} & 0_{3\times 3} \end{bmatrix} \in \mathbb{R}^{6\times 6}. \quad (19)$$

The only difference between P_{AE} and P_{KOE} is the block matrix P_{p}. Matrix (19) is used to constrain the positions on a 3D ellipsoid, while leaving the velocities unconstrained. When (19) is used in the BRSI computations, the resulting set represents all possible positions and velocities that enter the target set in some time-horizon. All of the resulting BRS are also (degenerate) ellipsoids.

Thus, given a union of BRSI, computed with (17), passive safety can be achieved by remaining in the safe set, $\mathbf{x} \in \mathcal{X}_{\mathrm{safe}}$, where

$$\mathcal{X}_{\mathrm{safe}} = \bar{\mathcal{R}}(t_k; \mathcal{S}_f, t_f)^c, \quad (20)$$

is the complement of the LTV BRSI (17). Clearly, enforcing the safe set directly as a constraint in an MPC problem, results in a non-convex optimization problem. In this work, $\bar{\mathcal{R}}(t_k; \mathcal{S}_f, t_f)$ is avoided by using separating hyperplanes near the exterior surface of the computed LTV BRSI. The hyperplanes are then used as linear constraints in an MPC policy which maintains the chaser spacecraft inside the safe set, i.e.,

$$\mathbf{x} \in \mathcal{X}_{\mathrm{safe}}, \ \forall t. \quad (21)$$

IV. Fail-safe Rendezvous Control

Next, we develop a fail-safe MPC policy that exploits the LTV BRSI (17). In particular, the MPC will use constraints to maintain the trajectory outside the BRSI while minimizing an appropriate cost function, for instance to reduce fuel consumption.

A. Constraints

In this work the MPC policy only enforces constraints that ensure passive safety. Additional constraints, e.g., on the control inputs, are straightforward to include. The constraints enforcing LTV BRSI (17) avoidance are non-convex, since they require avoiding a union of ellipsoids, i.e., $\mathbf{x} \notin \bar{\mathcal{R}}(t; \mathcal{S}_f, t_f)$. This significantly complicates the finite-horizon

MPC optimal control problem. In fact, even the avoidance of each ellipsoid is described by non-convex constraints,

$$\mathbf{x}^\top P_i^{-1}\mathbf{x} \geq 1. \tag{22}$$

Thus, here we implement a local convexification approach, based on computing a tangent to the constraints in the form of (22), and then enforcing half-space constraints to ensure that $\mathbf{x} \in \mathcal{X}_{\text{safe}}$.

The tangent hyperplanes are computed by projecting the state $\mathbf{x}$ radially onto the ellipsoids. The radial distance from the state to the surface of the ellipsoid $\mathcal{E}_i$ is

$$\rho^2 = \mathbf{x}^\top P_i^{-1}\mathbf{x}. \tag{23}$$

Normalizing the state $\mathbf{x}$ by ρ, results in the closest state on the ellipsoid surface

$$\mathbf{x}^{s_i} = \frac{\mathbf{x}}{\rho}. \tag{24}$$

The tangent hyperplane to the ellipsoid surface at $\mathbf{x}^{s_i}$ is defined by the normal vector

$$\mathbf{a}^i = 2P_i^{-1}\mathbf{x}^{s_i}, \tag{25}$$

since $P_i = P_i^\top$, so that the tangent hyperplane is

$$\{\mathbf{x} \in \mathbb{R}^6 : {\mathbf{a}^i}^\top \mathbf{x} = b^i\}, \tag{26}$$

where $b^i = {\mathbf{a}^i}^\top \mathbf{x}^{s_i}$.

Given a state $\mathbf{x}$ at time t, we compute projections $\mathbf{x}^{s_i}$ for all ellipsoids $\mathcal{E}_i \in \bar{\mathcal{R}}(t; \mathcal{S}_f, t_f)$. Due to the possibly large number of ellipsoids, rather than imposing half-space constraints for all of them, we only enforce the one that seems to be more conservative, i.e., the one that is most exterior to the center of the ellipsoids, in our case the origin, by selecting i such that

$$\mathbf{x}^{s_i *} = \arg\max_i \ ||\mathbf{x}^{s_i}||. \tag{27}$$

In the MPC policy, the hyperplanes are computed based on the previously predicted state trajectory. Let $(\mathbf{x}_{0|t-1} \dots \mathbf{x}_{N|t-1})$ be the trajectory computed at time $t-1$, where $\mathbf{x}_{k|t}$ denotes x predicted k steps ahead from t. Then, we can compute $\mathbf{a}_{k|t}$, $b_{k|t}$ from (24), (25) using $\mathbf{x}_{k+1|t-1}$ as prediction for $\mathbf{x}_{k|t}$

$$-\mathbf{a}_{k|t}^\top \mathbf{x}_{k|t} + b_{k|t} \leq s_{k|t}, \ k = 1, \dots, N \tag{28}$$

where N is the prediction horizon, and $s_k \geq 0$ is a slack variable softening constraints (28) to avoid infeasibility. For shortness we write (28) as

$$g_t(\mathbf{x}_{k|t}, \mathbf{u}_{k|t}, s_{k|t}) \leq 0. \tag{29}$$

B. Cost Function

The cost function of the MPC problem consists of a stage cost integrated along the prediction horizon and a terminal cost on the state at the end of the horizon, which encode the MPC control objectives. In this paper, the primary objective is for the rendezvous to occur, which amounts to the chaser spacecraft reaching and staying at the origin of the target orbital frame, i.e., reaching zero position and velocity. An additional objective is to minimize the total required propellant, since this allows for the increase of payload mass. This objective is encoded into the MPC policy by minimizing the thrust, $\mathbf{u}$, of the propulsion system. Finally, as the constraints derived from the LTV BRSI are softened, another objective of the controller is to minimize the safety constraint violations. Indeed, the safety and approach objectives are conflicting, resulting in trade-offs in the optimal solutions.

The stage cost is given by

$$F(\mathbf{x}, \mathbf{u}, s) = \mathbf{x}^\top Q\mathbf{x} + \mathbf{u}^\top R\mathbf{u} + w_s s^2, \tag{30}$$

where, $Q = Q^\top \geq 0$, $R = R^\top > 0$, $w_s \gg 0$.

The terminal cost is positive definite and quadratic. It encodes a penalty for not being at the desired zero-state by the end of the MPC window.

$$E(\mathbf{x}) = \mathbf{x}^\top M\mathbf{x}, \tag{31}$$

where $M = M^\top \geq 0$.

C. Optimal Control Problem

The MPC policy is based on solving a receding horizon optimal control problem of the following form

$$\begin{aligned} \min_{\mathbf{U}(t), \mathbf{s}_t} \quad & E(\mathbf{x}_{N|t}) + \sum_{k=0}^{N-1} F(\mathbf{x}_{k|t}, \mathbf{u}_{k|t}, s_{k|t}) \\ \text{s.t.} \quad & \mathbf{x}_{k+1|t} = A_d(t+k)\mathbf{x}_{k|t} + B_d\mathbf{u}_{k|t} \\ & \mathbf{x}_{0|t} = \mathbf{x}(t) \\ & g_t(\mathbf{x}_{k|t}, \mathbf{u}_{k|t}, s_{k|t}) \leq 0 \end{aligned} \tag{32}$$

where the prediction model for the MPC policy is given by (9), $\mathbf{s}_t = (s_{0|t} \dots s_{N-1|t})$ and $\mathbf{U}(t) = (\mathbf{u}_{0|t} \dots \mathbf{u}_{N-1|t})$. The resulting control policy is of the form,

$$\mathbf{u}(t) = \kappa_{mpc}(\mathbf{x}(t)) = \mathbf{u}^*_{0|t}, \tag{33}$$

where $\mathbf{u}^*_{0|t}$ is the first optimal control vector of the solution to (32).

D. Algorithm Overview

As mentioned earlier, the proposed approach is staged into three mission phases.

1) Phase 1: passive safety with respect to the AE.
2) Phase 2: passive safety with respect to the KOE.
3) Phase 3: no safety, final approach.

A summary of the fail-safe rendezvous control is found in Algorithm 1. Phase changes are triggered when the current state $\mathbf{x}(t)$ enters a bounding box $\mathcal{X}_{\text{box}_{\{\text{AE,KOE}\}}}$ around the AE or KOE, given by

$$\mathcal{X}_{\text{box}_{\{\text{AE,KOE}\}}} = \left\{ \mathbf{x} \in \mathbb{R}^6 \ : \ H\mathbf{x} \leq \begin{bmatrix} \mathbf{x}_{\lim} \\ \mathbf{x}_{\lim} \end{bmatrix}_{\{\text{AE,KOE}\}} \right\}, \tag{34}$$

where,

$$H = \begin{bmatrix} I_{3\times3} & \mathbf{0}_{3\times3} \\ -I_{3\times3} & \mathbf{0}_{3\times3} \end{bmatrix} \in \mathbb{R}^{6\times6}. \tag{35}$$

After the current state enters the KOE bounding box, an unconstrained $w_s = 0$ version of the optimal control problem (32) is solved to converge towards the target.

Algorithm 1 Fail-safe Rendezvous Control

Offline: Compute full AE and KOE LTV BRSI (17)

AE & KOE Approach

input: $\mathbf{x}(t)$
repeat
  Project $\mathbf{x}_{k|t}$ on all ellipsoids $\mathcal{E}_i \in \bar{\mathcal{R}}(t; \mathcal{S}_f, t_f)$ $\forall k$ (24)
  Select furthest hyperplanes from origin (27) $\forall k$
  Solve optimal control problem (32)
  Apply control policy (33) to the chaser spacecraft
until Spacecraft enters AE or KOE bounding Box (34)

Final Approach

input: $\mathbf{x}(t)$
repeat
  Solve optimal control problem (32)
  Apply control policy (33) to the chaser spacecraft
until Converged to the target

V. Simulation Results

To demonstrate the effectiveness of Algorithm 1 we consider an $\hat{\imath}_\theta$ (positive δx) approach where we compare the fail-safe control policy to a simulation where the passive safety constraints are removed. We measure control performance by total change in velocity as it is independent of satellite mass and thruster efficiency. The total ΔV of a maneuver is given by

$$\Delta V = \sum_{i=0}^{N-1} ||B\mathbf{u}_i|| \cdot \Delta t.$$

We consider a target in Earth-orbit with classical orbital elements given by

$$[a,\ e,\ i,\ \omega,\ \Omega,\ f]^\top = [7420\text{km},\ 0.1,\ 0.01°,\ 0°,\ 0°]^\top.$$

The resulting orbital period of the target body is $t_p = 106.02$ min $= 6361.2$ s. We define an AE around the target of size $\begin{bmatrix}1 & 2 & 1\end{bmatrix}$ km in the radial, along-track, and out-of-plane directions, and a KOE of size $\begin{bmatrix}100 & 200 & 100\end{bmatrix}$ m. The mass of the chaser spacecraft is $m_\text{c} = 4000$ kg.

The number of steps in the MPC horizon, the sampling period, the safety horizon, and the LTV BRSI (17) inflation factor are $N_\text{t} = 30$, $\Delta t = 30s$, $t_H = 2t_p$, and $\rho = 1.3$, respectively. All phases share the same state and control penalties in the stage cost, namely, $Q = I_6$, $R = 1.3 \cdot 10^4 I_3$. The terminal cost weight is $M = 10^2 I_6$. The slack variable penalty is $w_s = 10^6$ in the AE and KOE phases and $w_s = 0$ in the final approach phase.

In the following figure, the initial condition is represented by a blue circle, the blue trajectory is the relative position of the chaser with respect to the target, as seen in the target's orbital frame F_t. The black lines are sampled free-drift trajectories propagated forward without control to verify passive safety. We color the sampled free-drift trajectories red if they intersect either the AE or the KOE.

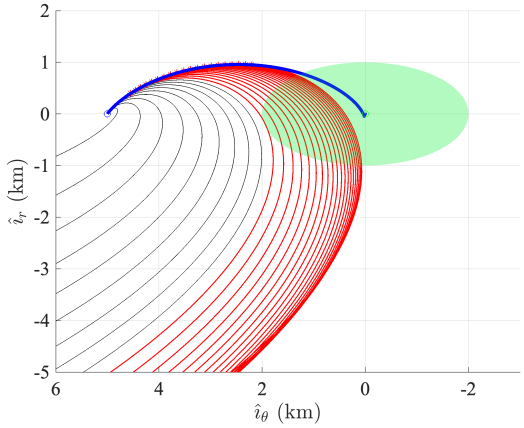

Fig. 2. $\hat{\imath}_\theta$ unsafe AE approach

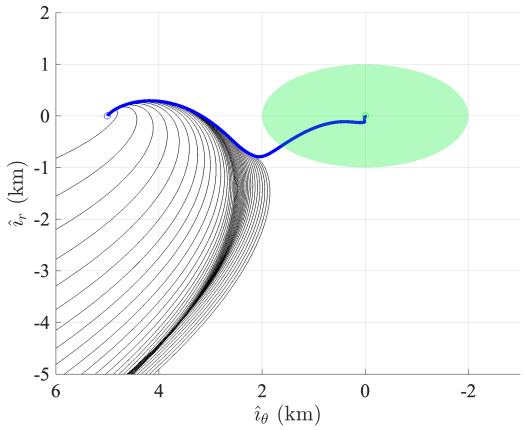

Fig. 3. $\hat{\imath}_\theta$ safe AE approach

We select an initial state $\mathbf{x}(0) = \begin{bmatrix}0 & 5 & 0 & 0 & 0 & 0\end{bmatrix}^\mathsf{T}$. As a baseline, we apply the MPC policy (33) with $w_s = 0$, that is, we do not enforce the passive safety constraints. The resulting maneuver is shown in Fig. 2 and requires $\Delta V_\text{unsafe} = 13.3631$ m/s. The spacecraft enters the AE LTV BRSI prior to reaching $\mathcal{X}_{box,\text{AE}}$, and thus, sampled free-drift trajectories along the nominal rendezvous maneuver intersect the AE and are unsafe (shown in red). Setting $w_s = 10^6$, we rerun the simulation and the resulting maneuver is shown in Fig. 3, requiring $\Delta V_\text{safe} = 20.5816$ m/s. The rendezvous maneuver is clearly modified due to the passive safety constraints, resulting in a passively safe trajectory towards the AE.

Once the chaser enters $\mathcal{X}_{\text{box,AE}}$, the maneuver proceeds towards the target while maintaining passive safety with respect to the KOE. The resulting maneuver is shown in Fig. 4. Figs. 5-6 show time histories of the control forces and a test of whether or not the current state is inside the LTV BRSI associated with the AE or the KOE. Phase switches between maintaining passive safety with respect to the AE, KOE, and the final approach phase are marked by vertical black lines. As seen in Fig. 6, the initial condition is actually

inside both the AE and KOE LTV BRSI. However, the fail-safe control policy of Algorithm 1 almost immediately guides the spacecraft outside of the LTV BRSI in order to maintain passive safety.

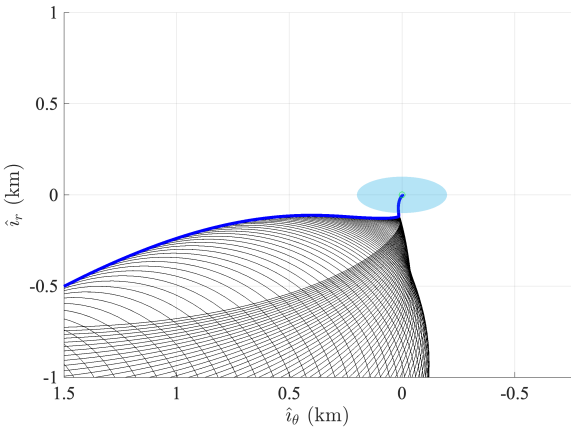

Fig. 4. $\hat{\imath}_\theta$ safe KOE approach

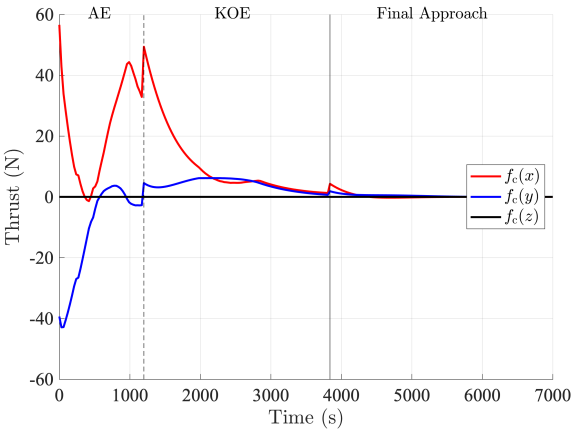

Fig. 5. $\hat{\imath}_\theta$ safe approach control

VI. CONCLUSIONS

The main contribution of this paper was the development of a fail-safe control policy for rendezvous on generic elliptic orbits using backwards reachable sets and model predictive control. The proposed control policy is able to satisfy passive safety constraints that, in the event of total thruster failure, keep a chaser spacecraft from colliding with a rendezvous target. In future work we will extend this method to also guarantee the existence of active safety abort maneuvers during final approach in the event of partial thruster failure when passive safety can no longer be guaranteed.

REFERENCES

[1] W. Fehse, *Automated rendezvous and docking of spacecraft*. Cambridge university press, 2003, vol. 16.

[2] L. S. Breger and J. P. How, "Safe trajectories for autonomous rendezvous of spacecraft," *J. Guidance, Control, and Dynamics*, vol. 31, no. 5, pp. 1478–1489, 2008.

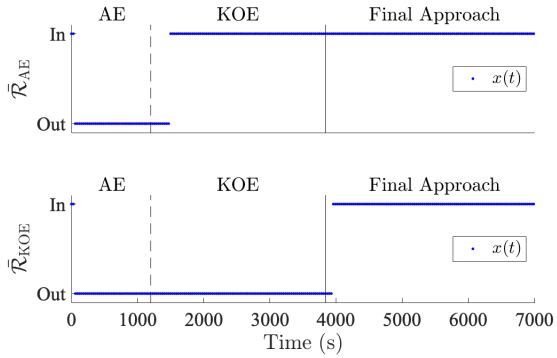

Fig. 6. $\hat{\imath}_\theta$ safe approach - state contained in AE and KOE LTV BRSI

[3] M. Holzinger, J. DiMatteo, J. Schwartz, and M. Milam, "Passively safe receding horizon control for satellite proximity operations," in *47th IEEE Conf. Decision and Control*, 2008, pp. 3433–3440.

[4] A. W. Koenig and S. D'Amico, "Robust and safe n-spacecraft swarming in perturbed near-circular orbits," *J. Guidance, Control, and Dynamics*, vol. 41, no. 8, pp. 1643–1662, 2018.

[5] M. Althoff, "An introduction to CORA 2015," in *Proc. Work. Applied Verification for Continuous and Hybrid Systems*, 2015.

[6] F. Borrelli, A. Bemporad, and M. Morari, *Predictive control for linear and hybrid systems*. Cambridge University Press, 2017.

[7] A. A. Kurzhanskiy and P. Varaiya, "Ellipsoidal techniques for reachability analysis of discrete-time linear systems," *IEEE Trans. Automatic Control*, vol. 52, no. 1, pp. 26–38, 2007.

[8] O. Maler, "Computing reachable sets: An introduction," *Tech. Rep. CNRS*, 2008.

[9] S. Bansal, M. Chen, S. Herbert, and C. J. Tomlin, "Hamilton-jacobi reachability: A brief overview and recent advances," in *56th Conf. Decision and Control*, 2017, pp. 2242–2253.

[10] M. J. Holzinger and D. J. Scheeres, "Reachability results for nonlinear systems with ellipsoidal initial sets," *IEEE trans. aerospace and electronic systems*, vol. 48, no. 2, pp. 1583–1600, 2012.

[11] C. Zagaris and M. Romano, "Reachability analysis of planar spacecraft docking with rotating body in close proximity," *J. Guidance, Control, and Dynamics*, vol. 41, no. 6, pp. 1416–1422, 2018.

[12] B. HomChaudhuri, M. Oishi, M. Shubert, M. Baldwin, and R. S. Erwin, "Computing reach-avoid sets for space vehicle docking under continuous thrust," in *55th Conf. Decision and Control (CDC)*, 2016, pp. 3312–3318.

[13] J. D. Gleason, A. P. Vinod, and M. M. Oishi, "Underapproximation of reach-avoid sets for discrete-time stochastic systems via lagrangian methods," in *56th Conf. Decision and Control (CDC)*, 2017.

[14] K. Lesser, M. Oishi, and R. S. Erwin, "Stochastic reachability for control of spacecraft relative motion," in *52nd Conf. Decision and Control*, 2013, pp. 4705–4712.

[15] M. Althoff, C. Le Guernic, and B. H. Krogh, "Reachable set computation for uncertain time-varying linear systems," in *Proc. 14th int. conf. Hybrid systems: computation and control*, 2011, pp. 93–102.

[16] B. P. Malladi, S. Di Cairano, and A. Weiss, "Nonlinear model predictive control of coupled rotational-translational spacecraft relative motion," in *American Control Conf.*, 2019, pp. 3581–3586.

[17] A. Weiss, M. Baldwin, R. S. Erwin, and I. Kolmanovsky, "Model predictive control for spacecraft rendezvous and docking: Strategies for handling constraints and case studies," *IEEE Trans. Control Systems Technology*, vol. 23, no. 4, pp. 1638–1647, 2015.

[18] S. Di Cairano, H. Park, and I. Kolmanovsky, "Model predictive control approach for guidance of spacecraft rendezvous and proximity maneuvering," *Int. J. Robust and Nonlinear Control*, vol. 22, no. 12, pp. 1398–1427, 2012.

[19] H. D. Curtis, *Orbital mechanics for engineering students*. Butterworth-Heinemann, 2013.

[20] A. B. Kurzhanski and P. Varaiya, "Ellipsoidal techniques for reachability analysis," in *Int. Work. on Hybrid Systems: Computation and Control*. Springer, 2000, pp. 202–214.

[21] M. Althoff, "Reachability analysis and its application to the safety assessment of autonomous cars," Ph.D. dissertation, Technische Universität München, 2010.